International Journal of Heat and Mass Transfer 52 (2009) 415–421

Contents lists available at ScienceDirect

International Journal of Heat and Mass Transfer

journal homepage: www.elsevier.com/locate/ijhmt

Unsteady mixed convection flow over a vertical wedge

Param Jeet Singh [a], S. Roy [a], R. Ravindran [b,*]

[a] Department of Mathematics, I.I.T. Madras, Chennai 600036, India
[b] Center for Differential Equations, Continuum Mechanics and Applications, School of Computational and Applied Mathematics, University of the Witwatersrand, Private Bag 3, Wits 2050, Johannesburg, South Africa

ARTICLE INFO

Article history:
Received 25 May 2007
Available online 25 July 2008

ABSTRACT

The behavior of unsteady mixed convection flow of an incompressible viscous fluid over a vertical wedge with constant suction/injection have been investigated. The unsteadiness is due to the time-dependent free stream velocity. The governing boundary layer equations along with the boundary conditions are first converted into dimensionless form by a non-similar transformation, and then resulting system of coupled non-linear partial differential equations is solved by an implicit finite-difference scheme in combination with the quasi-linearization technique. Numerical results for the effects of various parameters on velocity, temperature and concentration profiles and on their gradient at the wall are reported in the present study. The buoyancy force causes considerable velocity overshoot for low Prandtl number (Pr) fluids. Skin friction coefficient, heat and concentration transfer rates are found to alter significantly due to injection/suction for both accelerating and decelerating flow.

1. Introduction

Mixed convection flows over wedge shaped bodies are often encountered in many thermal engineering applications such as geothermal systems, crude oil extractions, ground water pollution, thermal insulation, heat exchanger and the storage of nuclear waste, etc. The system to be studied in the present investigation, shown schematically in Fig. 1, is a vertical wedge in a viscous fluid. If the temperature of the wedge surface and free stream differ, not only energy will be transferred to the flow but also density difference will exist. In a gravitational field, these density differences result an additional force, buoyancy force, beside viscous force due to viscous action. In many practical situations of moderate flow velocities and large fluid-wall temperature difference, the magnitude of buoyancy force and viscous force are of comparable order and convective heat transfer process is considered as mixed convection.

Free convection on an arbitrarily inclined plate with uniform surface heat flux was studied by Lin et al. [1]. In many investigations, notable contribution on convection flows over a vertical wedge was made by Watanabe [2], he is the first to study the thermal boundary layer over a wedge with uniform suction or injection in forced flow. Later, forced and free mixed convection boundary layer flow with uniform suction or injection on a vertical flat plate was studied again by Watanabe [3]. Further, Watanabe et al. [4] investigated the theoretical analysis on mixed convection boundary layer flow over a wedge with uniform suction or injection. In all the above problems the non-similar partial differential equations are transformed into ordinary differential equations by difference-differential method and the solutions of the resulting equations were obtained in the integral forms. Later, Yih [5] studied the MHD forced convection flow adjacent to a non-isothermal wedge. In this analysis, they considered the viscous dissipation and stress work on the MHD forced convection. Subsequently, Kumari et al. [6] investigated the mixed convection flow over a vertical wedge embedded in a highly porous medium. They solved the coupled non-linear partial differential equations by Keller box method. Recently, Jang et al. [7–9] have considered natural and mixed convection flows along vertical wavy surfaces. A simple coordinate transformation is employed to transform the complex wavy surface to a flat plate and marching finite-difference scheme is used for the analysis. All the above studies pertain to steady convection flows over a vertical inclined plate and wedge. Recently, finite-difference analysis of unsteady natural convection MHD flow past an inclined plate with variable surface heat and mass flux is studied by Ganesan et al. [10].

As a step towards the eventual development in the study of unsteady mixed convection flows, in the present investigation, it is proposed to obtain the non-similar solution for the unsteady mixed convection flow over a vertical wedge including the effects of suction/injection, semi-vertical angle and ratio of two buoyancy forces. The unsteadiness is introduced in the flow field by the time-dependent free stream velocity. The present study may have useful applications to several transport processes with surface mass transfer i.e. injection (or suction) crude oil extractions, ground water pollution, thermal insulation, heat exchanger and the storage of nuclear waste, etc. The non-similar solution of the coupled

* Corresponding author.
E-mail addresses: paramjeet@iitm.ac.in (P.J. Singh), Ravindran.Ramalingam@wits.ac.za (R. Ravindran).

0017-9310/$ - see front matter © 2008 Elsevier Ltd. All rights reserved.
doi:10.1016/j.ijheatmasstransfer.2008.06.014

Nomenclature

Roman letters

A	surface mass transfer parameter
C_{fx}	local skin friction coefficient
C	species concentration
f	dimensionless stream function
F	dimensionless velocity along x-direction
g	acceleration due to gravity
Gr_L, Gr_L^*	Grashoff numbers
k	thermal conductivity
m	pressure gradient parameter
Nu_x	local Nusselt number.
Pr	Prandtl number
$R(t^*)$	unsteady function of t^*
Re_L	Reynolds number
S	ratio of the buoyancy parameters
Sc	Schmidt number
Sh_x	local Sherwood number
t, t^*	dimensional and dimensionless time, respectively
T	temperature
u, v	axial and azimuthal velocity components
x, y	axial and vertical coordinates

Greek letters

α	thermal diffusivity
β, β^*	volumetric coefficient of thermal and concentration expansion, respectively
γ	vertical angle
ϵ	acceleration/deceleration parameter
η	similarity variable
θ	dimensionless temperature
λ, λ^*	buoyancy parameters
μ	dynamic viscosity
ν	kinematic viscosity
ξ	transformed axial coordinate
ρ	density
ϕ	dimensionless concentration
ψ	dimensional stream function

Subscripts

i, e, w, ∞	initial conditions, conditions in the free stream, at the wall and at infinity, respectively
ξ, η	denote the partial derivatives w.r.t. these variables, respectively
x, y	denote the partial derivatives w.r.t. these variable, respectively

non-linear partial differential equations governing the mixed convection flow has been obtained numerically using the quasi-linearization technique in combination with the implicit finite-difference scheme. The numerical results for some particular cases are matched with Watanabe et al. [4] and Kumari et al. [6] and found them in excellent agreement.

2. Analysis

Consider the unsteady mixed convection flow over a vertical wedge. The physical model and coordinate system are shown in Fig. 1. The axial coordinate x is measured along the surface and $x = 0$ corresponds to the leading edge of the wedge and y-axis is measured as the vertical distance from the surface. Thermophysical properties of the fluid in the flow model are assumed to be constant except the density variations causing a body force term in momentum equation. The Boussinesq approximation is invoked for the fluid properties to relate density changes to temperature changes, and to couple in this way the temperature field to the flow field [11]. Under the above assumptions, the equations of conservation of mass, momentum, energy and concentration governing the mixed convection boundary layer flow over a vertical wedge can be expressed as

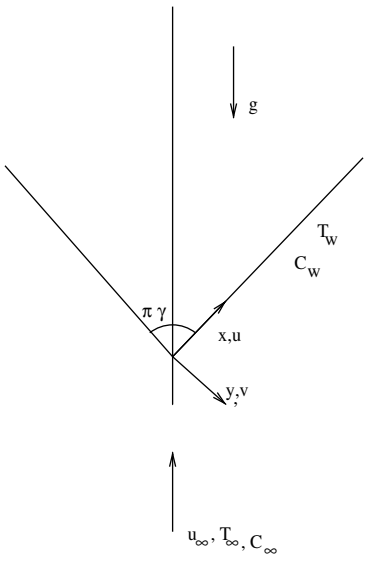

Fig. 1. Physical model and coordinate system.

$$\frac{\partial u}{\partial x}+\frac{\partial v}{\partial y}=0, \tag{1}$$

$$\frac{\partial u}{\partial t}+u\frac{\partial u}{\partial x}+v\frac{\partial u}{\partial y}=\frac{\partial u_e}{\partial t}+u_e\frac{\partial u_e}{\partial x}+\nu\left(\frac{\partial^2 u}{\partial y^2}\right)+[g\beta(T-T_\infty)+g\beta(C-C_\infty)]\cos\left(\frac{\pi\gamma}{2}\right), \tag{2}$$

$$\frac{\partial T}{\partial t}+u\frac{\partial T}{\partial x}+v\frac{\partial T}{\partial y}=\frac{\nu}{Pr}\left(\frac{\partial^2 T}{\partial y^2}\right), \tag{3}$$

$$\frac{\partial C}{\partial t}+u\frac{\partial C}{\partial x}+v\frac{\partial C}{\partial y}=\frac{\nu}{Sc}\left(\frac{\partial^2 C}{\partial y^2}\right). \tag{4}$$

The initial conditions are

$$\begin{aligned} &u(0,x,y)=u_i(x,y), \quad v(0,x,y)=v_i(x,y),\\ &T(0,x,y)=T_i(x,y), \quad C(0,x,y)=C_i(x,y), \end{aligned} \tag{5}$$

and the boundary conditions are given by

$$\begin{aligned} &u(t,x,0)=0, \quad v(t,x,0)=v_w(x,t), \quad T(t,x,0)=T_w=\text{Constant},\\ &C(t,x,0)=C_w=\text{Constant}, \quad u(t,x,\infty)=u_e(x,t), \quad v(t,x,\infty)=0,\\ &T(t,x,\infty)=T_\infty=\text{Constant}, \quad C(t,x,\infty)=C_\infty=\text{Constant}. \end{aligned} \tag{6}$$

Applying the following transformations:

$$\eta=\left[\frac{m+1}{2}\frac{u_e^*}{xv}\right]^{1/2}y,\quad \bar{x}=\frac{x}{L},\quad t^*=\frac{m+1}{2L}u_\infty(\bar{x})^m t,\quad u_e=u_e^*R(t^*),$$

$$u_e^*=u_\infty(\bar{x})^m,\quad m=\frac{\bar{x}}{u_e^*}\frac{\mathrm{d}u_e^*}{\mathrm{d}\bar{x}}=\frac{\gamma}{2-\gamma},\quad u=\psi_y,\quad v=-\psi_x,$$

$$\psi(t,x,y)=\left[\frac{2}{m+1}xvu_e^*\right]^{1/2}R(t^*)f(t^*,\bar{x},\eta),\quad \theta(t^*,\bar{x},\eta)=\frac{T-T_\infty}{T_w-T_\infty},$$

$$\phi(t^*,\bar{x},\eta)=\frac{C-C_\infty}{C_w-C_\infty},\quad u=u_ef_\eta(t^*,\bar{x},\eta)=u_e^*R(t^*)F,\quad \lambda=\frac{Gr_L}{Re_L^2},$$

$$f_\eta(t^*,\bar{x},\eta)=F(t^*,\bar{x},\eta),\quad Re_L=\frac{u_\infty L}{\nu},\quad Gr_L=\frac{g\beta L^3(T_w-T_\infty)\cos(\frac{\pi\gamma}{2})}{\nu^2},$$

$$Gr_L^*=\frac{g\beta^* L^3(C_w-C_\infty)\cos(\frac{\pi\gamma}{2})}{\nu^2},\quad \lambda^*=\frac{Gr_L^*}{Re_L^2},\quad S=\frac{\lambda^*}{\lambda},\quad N_1=\bar{x}\left(\frac{u_\infty}{u_e^*}\right)^2,$$

$$Pr=\frac{\nu}{\alpha},\quad Sc=\frac{\nu}{D},\quad -v_w\left[\frac{m+1}{2}\frac{x}{\nu u_e^*}\right]^{1/2}=R\left[\frac{m+1}{2}f_w+\bar{x}\frac{\partial f_w}{\partial\bar{x}}\right]+mt^*\left(R\frac{\partial f_w}{\partial t^*}+f_w\frac{\partial R}{\partial t^*}\right).\tag{7}$$

to Eqs. (1)–(4), we find that Eq. (1) is satisfied identically, and Eqs. (2)–(4) reduce to

$$F_{\eta\eta}+R\left[fF_\eta+\frac{2m}{m+1}(1-F^2)\right]+\frac{2\lambda N_1}{R(m+1)}(\theta+S\phi)+\frac{1}{R}\frac{\mathrm{d}R}{\mathrm{d}t^*}(1-F)-\frac{\partial F}{\partial t^*}=\frac{2R\bar{x}}{m+1}\left(F\frac{\partial F}{\partial\bar{x}}-F_\eta\frac{\partial f}{\partial\bar{x}}\right)+\frac{2Rmt^*}{m+1}\left(F\frac{\partial F}{\partial t^*}-F_\eta\frac{\partial f}{\partial t^*}\right)+\frac{2mt^*}{m+1}\frac{\mathrm{d}R}{\mathrm{d}t^*}F^2-\frac{2mt^*}{m+1}\frac{\mathrm{d}R}{\mathrm{d}t^*}(fF_\eta+1),\tag{8}$$

$$Pr^{-1}\theta_{\eta\eta}+Rf\theta_\eta-\frac{\partial\theta}{\partial t^*}=\frac{2R\bar{x}}{m+1}\left(F\frac{\partial\theta}{\partial\bar{x}}-\theta_\eta\frac{\partial f}{\partial\bar{x}}\right)+\frac{2mRt^*}{m+1}\left(F\frac{\partial\theta}{\partial t^*}-\frac{f\theta_\eta}{R}\frac{\mathrm{d}R}{\mathrm{d}t^*}-\theta_\eta\frac{\partial f}{\partial t^*}\right),\tag{9}$$

$$Sc^{-1}\phi_{\eta\eta}+Rf\phi_\eta-\frac{\partial\phi}{\partial t^*}=\frac{2R\bar{x}}{m+1}\left(F\frac{\partial\phi}{\partial\bar{x}}-\phi_\eta\frac{\partial f}{\partial\bar{x}}\right)+\frac{2mRt^*}{m+1}\left(F\frac{\partial\phi}{\partial t^*}-\frac{f\phi_\eta}{R}\frac{\mathrm{d}R}{\mathrm{d}t^*}-\phi_\eta\frac{\partial f}{\partial t^*}\right).\tag{10}$$

The boundary conditions reduce to

$$f_\eta(t^*,\bar{x},0)=0,\quad \theta(t^*,\bar{x},0)=1,\quad \phi(t^*,\bar{x},0)=1 \text{ at } \eta=0,$$
$$f_\eta(t^*,\bar{x},\eta_\infty)=1,\quad \theta(t^*,\bar{x},\eta_\infty)=0,$$
$$\phi(t^*,\bar{x},\eta_\infty)=0 \text{ at } \eta=\eta_\infty,\tag{11}$$

where η_∞ is the edge of the boundary layer and

$$f(t^*,\bar{x},\eta)=\int_0^\eta F\mathrm{d}\eta+f_w,\quad f_w=\frac{\bar{x}^{\frac{m+1}{2}}}{R}(t^{*2}\bar{x}^{2m}+A(m+1)^{1/2}\bar{x}),$$

and $A=-v_w\left(\frac{L}{2\gamma u_\infty}\right)^{1/2}=\text{Constant}$. If we put $\xi=\bar{x}^{(1-m)/2}$, then Eqs. (8)–(11) will reduce to the

$$F_{\eta\eta}+R\left[fF_\eta+\frac{2m}{m+1}(1-F^2)\right]+\frac{2\lambda N_2}{R(m+1)}(\theta+S\phi)+\frac{1}{R}\frac{\mathrm{d}R}{\mathrm{d}t^*}(1-F)-\frac{\partial F}{\partial t^*}=\frac{1-m}{m+1}R\xi\left(F\frac{\partial F}{\partial\xi}-F_\eta\frac{\partial f}{\partial\xi}\right)+\frac{2Rmt^*}{m+1}\left(F\frac{\partial F}{\partial t^*}-F_\eta\frac{\partial f}{\partial t^*}\right)+\frac{2mt^*}{m+1}\frac{\mathrm{d}R}{\mathrm{d}t^*}F^2-\frac{2mt^*}{m+1}\frac{\mathrm{d}R}{\mathrm{d}t^*}\left(fF_\eta+1\right),\tag{12}$$

$$Pr^{-1}\theta_{\eta\eta}+Rf\theta_\eta-\frac{\partial\theta}{\partial t^*}=\frac{1-m}{m+1}R\xi\left(F\frac{\partial\theta}{\partial\xi}-\theta_\eta\frac{\partial f}{\partial\xi}\right)+\frac{2mRt^*}{m+1}\left(F\frac{\partial\theta}{\partial t^*}-\frac{f\theta_\eta}{R}\frac{\mathrm{d}R}{\mathrm{d}t^*}-\theta_\eta\frac{\partial f}{\partial t^*}\right),\tag{13}$$

$$Sc^{-1}\phi_{\eta\eta}+Rf\phi_\eta-\frac{\partial\phi}{\partial t^*}=\frac{1-m}{m+1}R\xi\left(F\frac{\partial\phi}{\partial\xi}-\phi_\eta\frac{\partial f}{\partial\xi}\right)+\frac{2mRt^*}{m+1}\left(F\frac{\partial\phi}{\partial t^*}-\frac{f\phi_\eta}{R}\frac{\mathrm{d}R}{\mathrm{d}t^*}-\phi_\eta\frac{\partial f}{\partial t^*}\right).\tag{14}$$

The boundary conditions reduce to

$$f_\eta(t^*,\xi,0)=0,\quad \theta(t^*,\xi,0)=1,\quad \phi(t^*,\xi,0)=1 \text{ at } \eta=0,$$
$$f_\eta(t^*,\xi,\eta_\infty)=1,\quad \theta(t^*,\xi,\eta_\infty)=0,$$
$$\phi(t^*,\xi,\eta_\infty)=0 \text{ at } \eta=\eta_\infty,\tag{15}$$

where

$$N_2=\xi^{\frac{2(1-2m)}{1-m}},\quad f(t^*,\xi,\eta)=\int_0^\eta F\mathrm{d}\eta+f_w,$$

$$f_w=\frac{\xi^{\frac{m+1}{1-m}}}{R}\left(t^{*^2}\xi^{\frac{4m}{1-m}}+A(m+1)^{1/2}\xi^{\frac{2}{1-m}}\right)$$

and $A=-v_w\left(\frac{L}{2\gamma u_\infty}\right)^{1/2}=\text{Constant}$.

The local skin friction coefficient is given by

$$C_{fx}=\frac{2\mu}{\rho u_e^{*2}}\left(\frac{\partial u}{\partial y}\right)_{y=0}=R(t^*)[2(m+1)]^{1/2}Re_x^{-1/2}F_\eta(t^*,\xi,0),$$

$$\text{i.e. } Re_x^{\frac{1}{2}}C_{fx}=R(t^*)[2(m+1)]^{1/2}F_\eta(t^*,\xi,0).\tag{16}$$

The local heat transfer rate at the wall in terms of Nusselt number can be expressed as

$$Re_x^{-\frac{1}{2}}Nu_x=-\left(\frac{m+1}{2}\right)^{\frac{1}{2}}\theta_\eta(t^*,\xi,0),\tag{17}$$

where

$$Nu_x=\frac{-x\left[\frac{\partial T}{\partial y}\right]_{y=0}}{T_w-T_\infty}.$$

The local mass transfer rate at the wall in terms of Sherwood number can be expressed as

$$Re_x^{-\frac{1}{2}}Sh_x=-\left(\frac{m+1}{2}\right)^{\frac{1}{2}}\phi_\eta(t^*,\xi,0),\tag{18}$$

where

$$Sh_x=\frac{-x\left[\frac{\partial C}{\partial y}\right]_{y=0}}{C_w-C_\infty}.$$

The surface mass transfer parameter $A>0$ or $A<0$ according to whether there is suction/injection. It is assumed that the flow is unsteady due to the time-dependent free stream velocity $[u_e=u_e^*R(t^*)]$ where $R(t^*)=1+\epsilon t^{*2}$; $\epsilon>0$ or <0. Hence, the initial conditions are given by steady state equations obtained from Eqs. (12)–(14) by substituting $R(t^*)=1$, $\frac{\partial R}{\partial t^*}=\frac{\partial F}{\partial t^*}=\frac{\partial\theta}{\partial t^*}=\frac{\partial\phi}{\partial t^*}=0$, when $t^*=0$. The corresponding boundary conditions are obtained from Eq. (15) at $t^*=0$.

3. Results and discussion

The non-linear coupled partial differential Eqs. (12)–(14) under the boundary conditions given by Eq. (15) have been solved numerically using an implicit finite-difference scheme in combination with the quasi-linearization technique [12]. Since the method

is described for ordinary differential equations by Inouye and Tate [13] and also explained for partial differential equations in a recent study by Singh and Roy [14], its detailed description is not provided for the sake of brevity. In brief, an iterative sequence of linear equations are carefully constructed to approximate the non-linear Eqs. (12)–(14) achieving quadratic convergence and monotonicity. At each iteration step, the sequence of linear partial differential equations were expressed in difference form by using finite-difference scheme. Thus, in each iteration step, the resulting equations were then reduced to a system of linear algebraic equations with a block tri-diagonal matrix, which is solved by Varga's algorithm [15]. To ensure the convergence of the numerical solution to the exact solution, the step sizes $\Delta\eta$, $\Delta\xi$ and Δt^* have been optimized and taken as 0.01, 0.01 and 0.01, respectively. The results presented here are independent of the step sizes at least up to the fourth decimal place. A convergence criterion based on the relative difference between the current and previous iteration value is employed. When the difference reaches 10^{-4}, the solution is assumed to have converged and the iterative process is terminated.

In the present study, computations have been carried out for various values of $Pr(0.7 \leqslant Pr \leqslant 7.0)$, $A(-1.0 \leqslant A \leqslant 1.0)$, $\lambda(1.0 \leqslant \lambda \leqslant 10.0)$, $S(0.1 \leqslant S \leqslant 1.0)$, $m(0 \leqslant m \leqslant 0.33)$, and $Sc(0.22 \leqslant Sc \leqslant 2.57)$. The edge of the boundary layer (η_∞) has been taken between 3 and 5 depending on the values of the parameters. The unsteady free stream velocity distribution considered here are given by $R(t^*) = 1 + \epsilon t^{*2}$, where ϵ is constant and can be positive or negative. These velocity distributions represent accelerating/decelerating flows, respectively. To verify the correctness of our methods, we have compared some of our particular results with Watanabe et al. [4] and Kumari et al. [6]. The results are found in excellent agreement and some of the comparisons are shown in Tables 1 and 2.

The effects of buoyancy parameter (λ) and Prandtl number (Pr) on the velocity and temperature profiles (F, θ) for the accelerating flow $[R(t^*) = 1 + \epsilon t^{*2},\ \epsilon = 0.5]$ when $A = 1$, $Sc = 0.22$, $S = 0.1$ and $m = 0.2$ at $\xi = 1.0$ are displayed in Fig. 2. The buoyancy force (λ) shows the presence of overshoot in the velocity profile near the wall for lower Prandtl number fluid (Air, $Pr = 0.7$) but for higher Prandtl number fluid (Water, $Pr = 7.0$) the velocity overshoot is not observed. The magnitude of the overshoot increases with the buoyancy parameter (λ) but decreases as the Prandtl number increases. The reason is that the buoyancy force (λ) affects more in low Prandtl number fluid (Air, $Pr = 0.7$) due to the low viscosity of the fluid (Air, $Pr = 0.7$), which increases the velocity within the boundary layer as the assisting buoyancy force acts like a favorable pressure gradient. Hence, the velocity overshoot occurs and for higher Prandtl number fluids the overshoot is not observed because higher Prandtl number (Water, $Pr = 7.0$) implies more viscous fluid which makes it less sensitive to the buoyancy

Table 1
Comparison of steady-state results $(F_\eta(\xi,0), -\theta_\eta(\xi,0))$ when $m = 0.0909$, $N_2 = 1$ and $Pr = 0.73$ with those of Watanabe et al. [4]

A	Present results		Watanabe et al. [4]	
	$F_\eta(\xi,0)$	$-\theta_\eta(\xi,0)$	$F_\eta(\xi,0)$	$-\theta_\eta(\xi,0)$
−2.5	0.42570	0.00105	0.42558	0.00095
−2.0	0.53518	0.00721	0.53488	0.00697
−1.5	0.71007	0.03395	0.70991	0.03362
−1.0	0.98585	0.1188	0.98579	0.11265
−0.5	1.37930	0.28188	1.37927	0.28175
0.0	1.87410	0.56594	1.87405	0.56590
0.5	2.43952	0.96931	2.43933	0.96952
1.0	3.05551	1.47811	3.05506	1.47859
1.5	3.71989	2.06570	3.71904	2.06640
2.0	4.43651	2.70142	4.43591	2.70217
2.5	5.20535	3.36068	5.20427	3.36068

Table 2
Comparison of steady-state results $(F_\eta(\xi,0), -\theta_\eta(\xi,0))$ when $\lambda = 0$, $A = 0$ and $Pr = 0.73$ with those of Kumari et al. [6]

m	Present results		Kumari et al. [6]	
	$F_\eta(\xi,0)$	$-\theta_\eta(\xi,0)$	$F_\eta(\xi,0)$	$-\theta_\eta(\xi,0)$
0	0.46975	0.42046	0.46975	0.42079
0.0141	0.50481	0.42606	0.50472	0.42635
0.0435	0.56895	0.43559	0.56904	0.43597
0.0909	0.65490	0.44742	0.65501	0.44770
0.1429	0.73196	0.45705	0.73202	0.45728
0.2000	0.80208	0.46511	0.80214	0.46534
0.3333	0.92767	0.47815	0.92766	0.47840

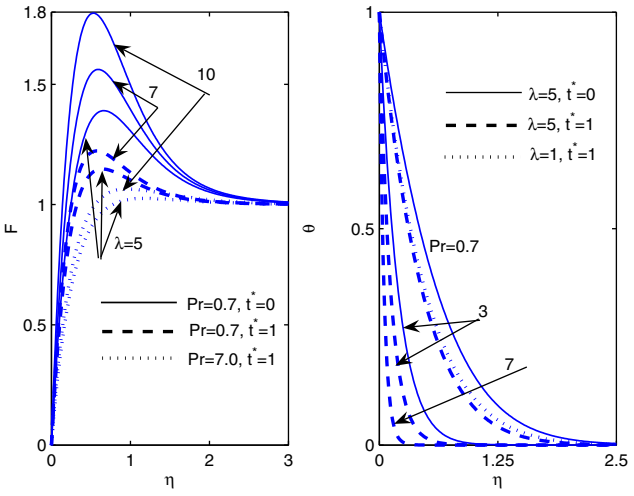

Fig. 2. Effects of λ and Pr on F and θ for accelerating flow $[R(t^*) = 1 + \epsilon t^{*2}, \epsilon = 0.5]$ when $S = 0.1$, $m = 0.2$, $Sc = 0.22$, $A = 1$ at $\xi = 1.0$.

parameter (λ). The time effect is crucial for the velocity overshoot. For example, for $\epsilon = 0.5$, $A = 1$, $\lambda = 5$, $S = 0.1$ at $\xi = 1.0$, overshoot in the velocity (F) profile reduced approximately by 18% as t^* increases from 0 to 1. The effect of λ is comparatively less in temperature profile (θ) as shown in Fig. 2. Moreover, Fig. 2 also shows that the effect of higher Prandtl number (Pr) results into the thinner thermal boundary layer as the higher Prandtl number fluid (Water, $Pr = 7.0$) has a lower thermal conductivity. The effect of Prandtl number (Pr) is very less in concentration profile as shown in Fig. 3. Fig. 3 also shows the effect of higher Schmidt number (Sc) results into the thinner concentration boundary layer as higher Schmidt number (Sc) fluid has a lower concentration diffusivity.

The effects of buoyancy parameter (λ) and Prandtl number (Pr) on skin friction coefficient ($C_{fx}Re_x^{1/2}$) for accelerating and decelerating free stream flows $[R(t^*) = 1 + \epsilon t^{*2},\ \epsilon = 0.5 \text{ and } -0.5]$ are shown in Fig. 4. The skin friction coefficient ($C_{fx}Re_x^{1/2}$) increases with the buoyancy parameter λ. The physical reason is that the positive buoyancy force ($\lambda > 0$) implies favorable pressure gradient, and the fluid gets accelerated, which results in thinner momentum boundary layer. Consequently, the local skin friction ($C_{fx}Re_x^{1/2}$) is also increased at all times. Skin friction coefficient ($C_{fx}Re_x^{1/2}$) decrease with the increase of Prandtl number (Pr). The reason for this trend is that the higher Prandtl number (Pr) fluid means more viscous fluid, which increase the boundary layer thickness and consequently, reduce the shear stress. For example, for $\epsilon = 0.5$, $S = 0.1$, $A = 1$, $Sc = 0.22$, $m = 0.2$ and $\xi = 1$ at time $t^* = 1$, Fig. 4 shows that the percentage increase in skin friction coefficient ($C_{fx}Re_x^{1/2}$) are approximately 48% and 12% when λ changes from 1 to 5 and Prandtl number (Pr) changes from 7 to 0.7, respectively.

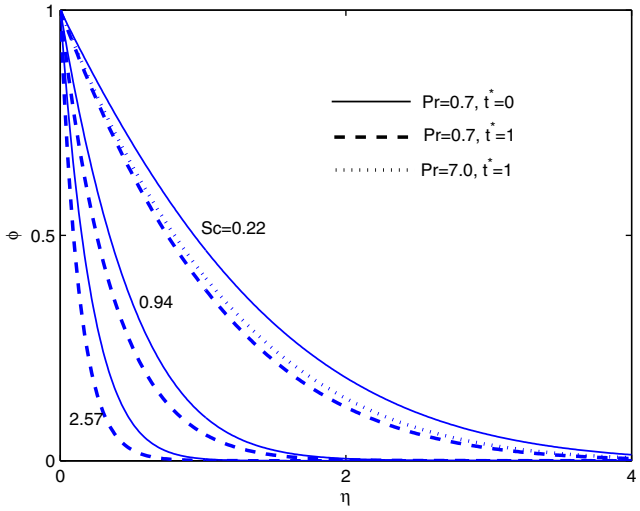

Fig. 3. Effects of Pr and Sc on ϕ for accelerating flow $[R(t^*) = 1 + \epsilon t^{*2}, \epsilon = 0.5]$ when $S = 0.1$, $m = 0.2$, $\lambda = 5$ and $A = 1$ at $\xi = 1.0$.

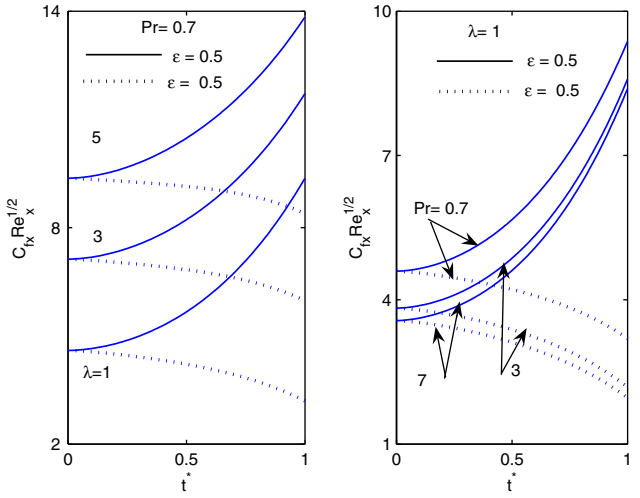

Fig. 4. Effects of λ and Pr on $C_{fx}Re_x^{1/2}$ for accelerating and decelerating flows $[R(t^*) = 1 + \epsilon t^{*2}, \epsilon = 0.5$ and $-0.5]$ when $m = 0.2$, $S = 0.1$, $Sc = 0.22$ and $A = 1$ at $\xi = 1.0$.

The effects of suction $(A > 0)$ and injection $(A < 0)$ parameter on the velocity and temperature profiles (F, θ) when $Pr = 0.7$, $Sc = 0.22$, $\lambda = 1$, $\epsilon = 0.5$, $m = 0.2$ and $S = 0.1$ at $\xi = 1$ are shown in Fig. 5. In case of injection, the fluid is carried away from the surface, causing reduction in the velocity gradient as it tries to maintain the same velocity over a very small region near the surface, and this effect is reversed in the case of suction. The higher velocity overshoot is observed near the wall within the boundary layer for injection $(A < 0)$ and overshoot is decreased for suction $(A > 0)$. Injection $(A < 0)$ causes a decrease in the steepness of the velocity profile (F) near the wall within the boundary layer, but the steepness of the velocity profile (F) increases with suction. With a decrease in the suction parameter which correspond to either increasing injection or decreased suction, the temperature profiles swell. On the other hand, as the parameter A is decreased, the maximum velocity increases and location of η at maximum velocity shifts away from the wall. The effects of injection $(A < 0)$ and suction $(A > 0)$ on the skin friction and heat transfer coefficients $(C_{fx}Re_x^{1/2},\ Nu_xRe_x^{-1/2})$ are shown in Fig. 6. As expected, results indicate that skin friction and heat transfer coefficients $(C_{fx}Re_x^{1/2},\ Nu_xRe_x^{-1/2})$ increase with the in-

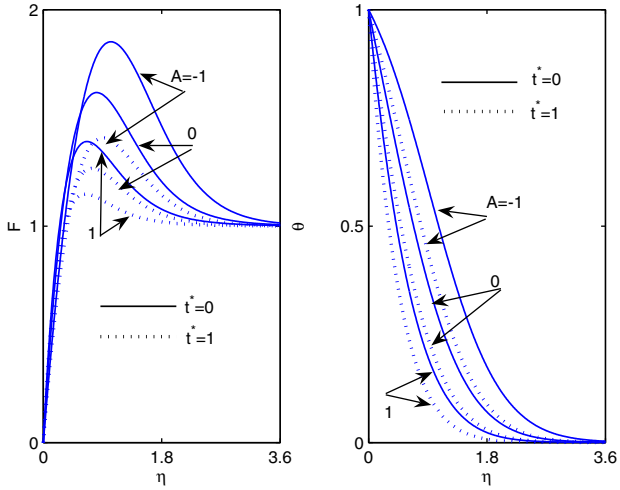

Fig. 5. Effect of A on F and θ for accelerating flow $[R(t^*) = 1 + \epsilon t^{*2}, \epsilon = 0.5]$ when $\lambda = 5$, $Pr = 0.7$, $S = 0.1$, $m = 0.2$ and $Sc = 0.22$ at $\xi = 1.0$.

crease of suction parameter $(A > 0)$ but decrease as the magnitude of injection $(A < 0)$ increase. Fig. 6 also shows that the skin friction coefficient $(C_{fx}Re_x^{1/2})$ increases for the accelerating flow and decreases for the decelerating flow with the increase of time t^*. On the other hand, heat transfer parameter i.e. Nusselt number $(Nu_xRe_x^{-1/2})$ increases for both accelerating and decelerating flows with the increase of time t^*. However, the rate of increase in Nusselt number $(Nu_xRe_x^{-1/2})$ with time t^* is much less for decelerating flow as compared to the accelerating flow. The physical reason is that the higher friction between wedge surface and fluid flow generates more heat for the case of accelerating flow. Fig. 7 displays the injection $(A < 0)$ and suction $(A > 0)$ parameter effect on the concentration profile and Sherwood number $(\phi,\ Sh_xRe_x^{-1/2})$ when $Pr = 0.7$, $Sc = 0.22$ and $m = 0.2$ at $\xi = 1$. Results indicate that due to the decrease in the suction parameter which correspond to either increasing injection or decreasing suction, the concentration profiles swell. The effect of injection $(A < 0)$ and suction $(A > 0)$ on the concentration coefficient i.e. Sherwood number $(Sh_xRe_x^{-1/2})$ is also shown in Fig. 7. As expected, results indicate that concentra-

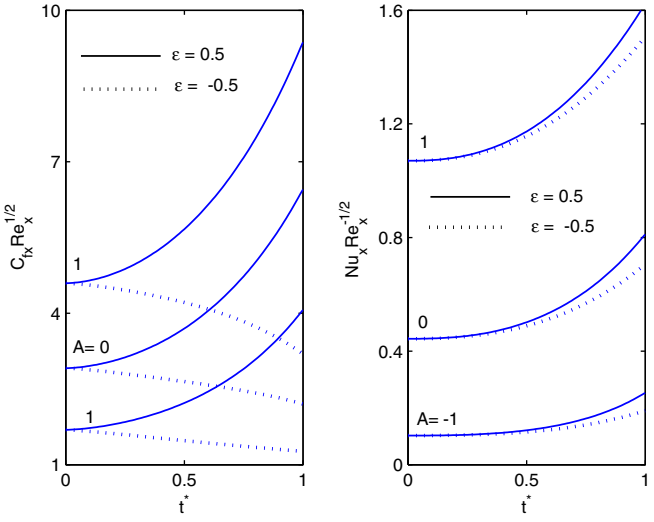

Fig. 6. Effect of A on the $C_{fx}Re_x^{1/2}$ and $Nu_xRe_x^{-1/2}$, for accelerating and decelerating flows $[R(t^*) = 1 + \epsilon t^{*2}, \epsilon = 0.5$ and $-0.5]$ when $\lambda = 1$, $m = 0.2$, $S = 0.2$, $Sc = 0.22$ and $Pr = 0.7$ at $\xi = 1.0$.

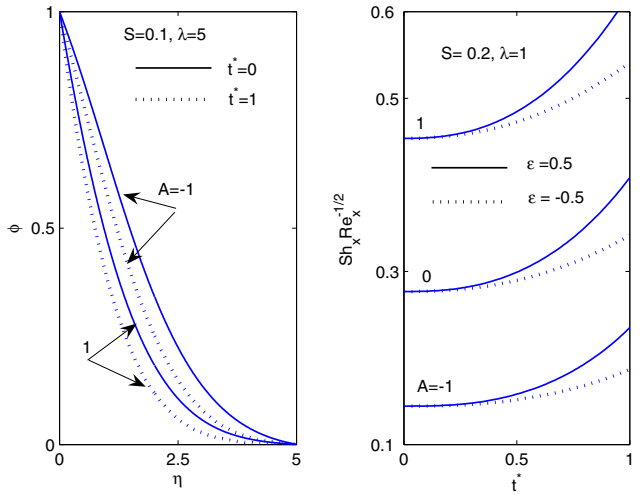

Fig. 7. Effect of A on ϕ for accelerating flow $[R(t^*) = 1 + \epsilon t^{*2}, \epsilon = 0.5]$ and on $Sh_x Re_x^{-1/2}$ for accelerating and decelerating flows $[R(t^*) = 1 + \epsilon t^{*2}, \epsilon = 0.5$ and $-0.5]$ when $m = 0.2$, $Sc = 0.22$ and $Pr = 0.7$ at $\xi = 1.0$.

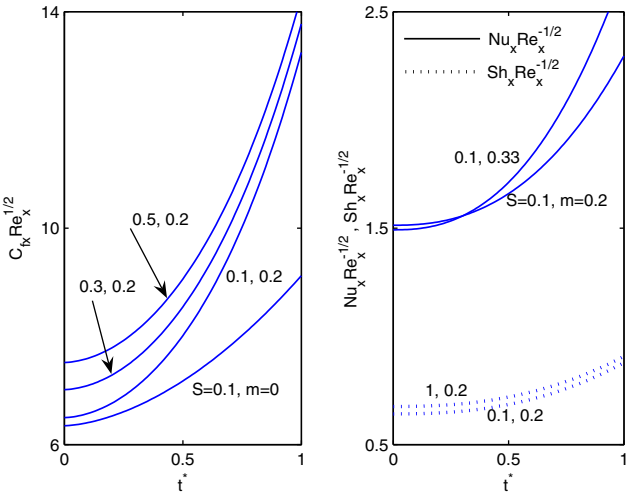

Fig. 9. Effects of S and m on the $C_{fx}Re_x^{1/2}$, $Nu_xRe_x^{-1/2}$ and $Sh_xRe_x^{-1/2}$ for accelerating flow $[R(t^*) = 1 + \epsilon t^{*2}, \epsilon = 0.5]$ when $\lambda = 5$, $A = 1$, $Sc = 0.22$ and $Pr = 0.7$ at $\xi = 1.0$.

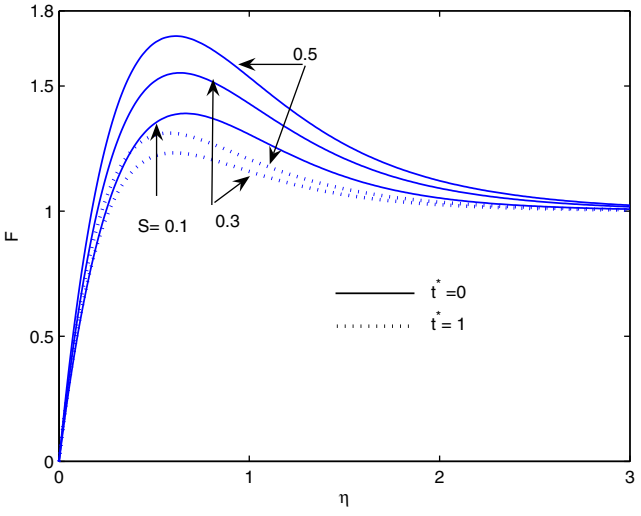

Fig. 8. Effect of S on F for accelerating flow $[R(t^*) = 1 + \epsilon t^{*2}, \epsilon = 0.5]$ when $\lambda = 5$, $m = 0.2$, $Pr = 0.7$, $Sc = 0.22$, $A = 1$ at ξ=1.0.

tion coefficient i.e. Sherwood number ($Sh_xRe_x^{-1/2}$) increases with the increase of suction parameter ($A > 0$) but decreases as the magnitude of injection ($A < 0$) increases. Sherwood number ($Sh_xRe_x^{-1/2}$) increases with time t^* for accelerating flow as well as for decelerating flow but the rate of increase in decelerating flow is much less as compared to accelerating flow.

Fig. 8 presents the effect of S (ratio of concentration buoyancy force to thermal buoyancy force parameters) on the velocity profile (F) when $\lambda = 5$, $Pr = 0.7$, $Sc = 0.22$, $A = 1$ and $m = 0.2$ at $\xi = 1$. The positive values of S implies that both buoyancy forces act in the same direction and it has been observed that the magnitude of velocity increases with the increase of S ($S > 0$). The physical reason is that the assisting buoyancy force due to thermal and concentration gradients acts like a favorable pressure gradient which accelerates the fluid for low Prandtl number (Air, $Pr = 0.7$) causing the velocity overshoot within the boundary layer. The velocity overshoot reduces as time increases. The effects of S and pressure gradient parameter (m) on the skin friction coefficient ($C_{fx}Re_x^{1/2}$), Nusselt Number ($Nu_xRe_x^{-1/2}$) and Sherwood number ($Sh_xRe_x^{-1/2}$) when $\lambda = 1$, $Pr = 0.7$, $Sc = 0.22$ and $A = 1$ at $\xi = 1$ are shown in Fig. 9. Due to the increase in S, the skin friction coefficient ($C_{fx}Re_x^{1/2}$) and Sherwood number ($Sh_xRe_x^{-1/2}$) increase as can be seen in Fig. 9. The effect of S on the temperature and concentration profiles is very less because S parameter is explicitly present only in the momentum equation and those profiles are not shown for the sake of brevity. Results indicate that skin friction and heat transfer coefficients ($C_{fx}Re_x^{1/2}$, $Nu_xRe_x^{-1/2}$) increase with the increase of pressure gradient parameter (m). In particular at time $t^* = 1$, the percentage increase in the skin friction coefficient ($C_{fx}Re_x^{1/2}$) is 45% when m changes from 0 to 0.2 and in heat transfer parameter ($Nu_xRe_x^{-1/2}$) is 17%, when m changes from 0.2 to 0.33 for $A = 1$, $Pr = 0.7$, $Sc = 0.22$, $S = 0.1$, $\lambda = 1$ and $\xi = 1$. It may be noted that the pressure gradient parameter (m) is explicitly present in the expressions of skin friction, heat and mass transfer coefficients ($C_{fx}Re_x^{1/2}$, $Nu_xRe_x^{-1/2}$, $Sh_xRe_x^{-1/2}$).

4. Conclusions

A detailed numerical study has been carried out for the unsteady mixed convection over a vertical wedge. Conclusions of the study are as follows:

- The buoyancy force causes overshoot in the velocity profile for low Prandtl number fluid (Air, $Pr = 0.7$) and overshoot reduces significantly as t^* increases. The effect of buoyancy force on the temperature and concentration profiles are not significant.
- Higher Prandtl number ($Pr = 7$) causes thinner thermal boundary layer and higher Schmidt number ($Sc = 2.57$) causes thinner concentration boundary layer.
- The buoyancy force, ratio of two buoyancy forces and pressure gradient parameter strongly affects the skin friction coefficient, whereas as the effect of these parameters on Nusselt and Sherwood numbers is not significant.
- Skin friction coefficient, heat and concentration transfer rate are found to alter significantly due to injection/suction ($-1 \leqslant A \leqslant 1.0$) for both accelerating and decelerating free stream flows.
- Skin friction, heat transfer and mass transfer coefficients are strongly affected by the time-dependent free stream velocity which confirms the importance of present investigation of unsteady mixed convection flow.

References

[1] H.T. Lin, W.S. Yu, S.L. Yang, Free convection on an arbitrarily inclined plate wait uniform surface heat flux, Warme Stoffubertragung 24 (1989) 183–190.
[2] T. Watanabe, Thermal boundary layers over a wedge with uniform suction or injection in forced flow, Acta Mech. 83 (1990) 119–126.
[3] T. Watanabe, Forced and free mixed convection boundary layer flow with uniform suction or injection on a vertical plate, Acta Mech. 89 (1991) 123–132.
[4] T. Watanabe, K. Funazaki, H. Taniguchi, Theoretical analysis on mixed convection boundary layer flow over a wedge with uniform suction or injection, Acta Mech. 105 (1994) 133–141.
[5] K.A. Yih, MHD forced convection flow adjacent to a non-isothermal wedge, Int. Commun. Heat Mass Transfer 26 (1999) 819–827.
[6] M. Kumari, H.S. Takhar, G. Nath, Mixed convection flow over a vertical wedge embedded in a highly porous media, Heat Mass Transfer 37 (2001) 139–146.
[7] J.-H. Jang, W.-M. Yan, H.C. Liu, Natural convection heat and mass transfer along a vertical wavy surface, Int. J. Heat Mass Transfer 46 (2003) 1075–1083.
[8] Jer-Huan Jang, Wei-Mon Yan, Mixed convection heat and mass transfer along a vertical wavy surface, Int. J. Heat Mass Transfer 47 (2004) 419–428.
[9] J.-H. Jang, W.-M. Yan, Transient analysis of heat and mass transfer by natural convection over a vertical wavy surface, Int. J. Heat Mass Transfer 47 (2004) 3695–3705.
[10] P. Ganesan, G. Palani, Finite difference analysis of unsteady natural convection MHD flow past an inclined plate with variable surface heat and mass flux, Int. J. Heat Mass Transfer 47 (2004) 4449–4457.
[11] H. Schlichting, Boundary Layer Theory, Springer, New York, 2000.
[12] R.E. Bellman, R.E. Kalaba, Quasilinearization and Non-linear Boundary Value Problem, Elsevier, USA, 1965.
[13] K. Inouye, A. Tate, Finite difference version quasilinearization applied to boundary layer equations, AIAAJ 12 (1974) 558–560.
[14] P.J. Singh, S. Roy, Unsteady mixed convection flow over a vertical cone due to impulsive motion, Int. J. Heat Mass Transfer 50 (2007) 949–959.
[15] R.S. Varga, Matrix Iterative Analysis, Prentice Hall, 2000.